Int. J. Non-Linear Mechanics, Vol. 27, No. 5, pp. 861–874, 1992
Printed in Great Britain.

0020–7462/92 $5.00 + .00
Pergamon Press Ltd

NORMAL MODES AND GLOBAL DYNAMICS OF A TWO-DEGREE-OF-FREEDOM NON-LINEAR SYSTEM—I. LOW ENERGIES

A. F. VAKAKIS

Department of Mechanical and Industrial Engineering, University of Illinois at Urbana-Champaign, Urbana, IL 61801, U.S.A.

and

R. H. RAND

Department of Theoretical and Applied Mechanics, Cornell University, Ithaca, NY 14853, U.S.A.

(*Received* 23 *January* 1991; *in revised form* 3 *June* 1991)

Abstract—The global dynamics of an undamped, strongly non-linear, two-degree-of-freedom system are analyzed by means of *Poincaré* maps. The oscillator under consideration contains "similar" non-linear normal modes and at certain values of its structural parameters a mode bifurcation is possible. The effect of this bifurcation on the global dynamics is investigated by numerical and analytical techniques. For low energies, a homoclinic orbit exists in the Poincaré map, and is approximately analyzed by the two-variable expansion method. This homoclinic orbit is exclusively caused by the similar mode bifurcation, and as shown in a companion paper [A. K. Vakakis and R. H. Rand, *Int. J. Non-Linear Mech.* **27**, 875–888 (1992)] it gives rise to large-scale chaotic motions when the energy is increased.

1. INTRODUCTION

For n-degree-of-freedom (DOF) Hamiltonian systems there exist basic theorems by Liapounov [2] and Weinstein [3], stating that for each fixed level of energy there exists *at least* n-periodic solutions (normal modes) passing through each stable equilibrium. Moreover, some of these solutions may not be analytic continuations of linear normal modes.

Rosenberg in a series of papers [4–6] provided analytical methods for computing normal modes. In his work, both "similar" and "nonsimilar" normal modes were computed and their stability was analyzed by linearized stability techniques. An interesting feature of the free oscillations of strongly non-linear systems is that the number of non-linear normal modes may exceed the number of DOF of the oscillator [6]. This is because non-linear mode bifurcations can occur, increasing in complexity as the degree of non-linearity increases [7]. Methods for studying the mode bifurcations and stability can be found in the literature [7–11]. In these works the local dynamics of the non-linear system were examined in sufficiently small neighborhoods of the normal modes, by a variety of approximate numerical and analytical techniques.

Although the existing linearized local techniques presented in these references can capture to a large extend the real dynamics of the system sufficiently close to the normal mode, they have two inherent deficiencies. First, they cannot describe the global dynamics of the oscillator away from the normal modes. Then, there are cases where linearized techniques cannot even capture the local dynamics. Such a case is reported in ref. [12] where a symmetric system with cubic non-linearity is examined. For that system, a linearized, Mathieu-type stability analysis cannot even determine the local stability of the symmetric mode of the system. The cause for this stability indeterminacy is discussed in ref. [13], and in refs [13–15], improved analytical methodologies for detecting the local mode stability are presented.

This is done by applying Poincaré maps to the study of the local dynamics in neighborhoods of the normal modes [13–15]. In these references, analytic techniques for approximating the Poincaré maps in low energies (such as Birkhoff–Gustavson canonical transformations, Whittaker's adelphic integrals and Lie transforms), are given. By applying these

techniques, one can determine analytically the local flow of the dynamical system sufficiently close to a normal mode, and thus obtain a more complete description of the mode stability.

In this work, the global dynamics of an oscillator with cubic non-linearity will be considered. Both numerical and analytical methods will be applied to the study of the low dynamics. The implications of the bifurcation of normal modes on the global dynamics will be investigated: it will be shown that the mode bifurcation leads to the creation of a homoclinic orbit which for high energies gives rise to large-scale chaotic free motions [1]. After a brief review of Poincaré maps in Section 2, we apply numerical simulation and perturbation analysis to nearly linear (low energy) dynamics in Section 3. Finally, in Section 4, the main findings of the work are discussed.

2. POINCARÉ MAPS

In this section a brief description of the construction of the Poincaré map is given. Consider the DOF undamped system of Fig. 1, containing stiffnesses with cubic non-linearity. The equations of free motion of this system are given by

$$\ddot{x}_1 + x_1 + x_1^3 + K(x_1 - x_2)^3 = 0 \tag{1a}$$

$$\ddot{x}_2 - K(x_1 - x_2)^3 + x_2 + x_2^3 = 0. \tag{1b}$$

The system is Hamiltonian with a four-dimensional phase space $(x_1, \dot{x}_1, x_2, \dot{x}_2)$. The global dynamics of this system was first studied by Month and Rand [12–15], by constructing Poincaré maps. Here only a brief description of the constuction of these maps will be given and for a more detailed discussion, the reader is referred to the aforementioned references.

By fixing the total energy of the system to a constant level, one restricts the flow of this dynamical system to an isoenergetic three-dimensional manifold. This is done by setting:

$$H(x_1, \dot{x}_1, x_2, \dot{x}_2) = h \tag{2}$$

or,

$$H(x_1, \dot{x}_1, x_2, \dot{x}_2) = \tfrac{1}{2}(x_1^2 + x_2^2) + \tfrac{1}{4}[x_1^4 + x_2^4 + K(x_1 - x_2)^4] + \tfrac{1}{2}(\dot{x}_1^2 + \dot{x}_2^2) = h \tag{3}$$

where $H(\cdot)$ is the Hamiltonian of the system, and h is the constant energy level. The Hamiltonian H is a first integral of motion, and for autonomous oscillators it represents conservation of energy during free oscillations. If an additional independent first integral of motion exists, the two-DOF system is said to be "integrable" and the isoenergetic manifold $H = h$ is fibered by invariant two-dimensional tori [16]. This "integrability" property is not generic in Hamiltonian systems and in general, one does not expect the existence of a second integral of motion. (In fact, the integrable cases are of measure zero in the "space" of this class of non-linear systems.) It must be noted, however, that for low energies even non-integrable oscillators appear to have an "approximate" second integral of motion. This is because for low amplitudes their isoenergetic manifolds appear to be fibered by approximate invariant tori which, as the energy increases, "break" giving rise to random-like chaotic motions [17].

Now suppose that one intersects the three-dimensional isoenergetic manifold defined by equations (2) and (3), with a two-dimensional cut plane. If the intersection of the two manifolds is transverse [16], the resulting cross-section Σ is two-dimensional, and the flow

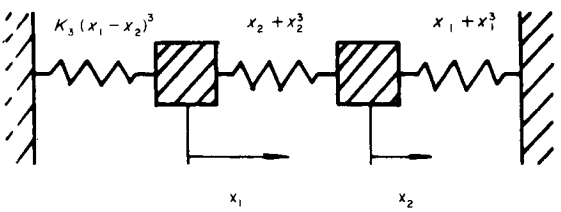

Fig. 1. The non-linear oscillator under consideration.

of the dynamical system intersecting the cut plane defines a "Poincaré map". A schematic representation of a Poincaré map is shown at Fig. 2, where the cut plane is chosen as

$$T: \{x_1 = 0\} \tag{4}$$

and the Poincaré section Σ is defined by

$$\Sigma = \{x_1 = 0, \dot{x}_1 > 0\} \cap \{H = h\}. \tag{5}$$

Note that an additional restriction on the sign of the velocities of the intersecting points was posed. This is because one requires the Poincaré map to be orientation preserving [16] (in Fig. 2 this is done by recording only points A and A′, but not point B which corresponds to a negative velocity at the point of intersection). Also note that transverse intersections of the flow with the cut plane will only occur if the following condition is satisfied:

$$(\dot{x}_1, \ddot{x}_1, \dot{x}_2, \ddot{x}_2) \cdot (1, 0, 0, 0) \neq 0 \Rightarrow \dot{x}_1 \neq 0. \tag{6}$$

A free motion of the system corresponding to a normal mode is a periodic orbit and therefore pierces the cut-section only once. As a result, the Poincaré section, Σ, of a normal mode is a single point and the mode stability can be determined by examining the Poincaré sections of "near-by" trajectories (corresponding to initial conditions that are very close to those of the normal mode). If the point corresponding to the normal mode appears as a center, i.e. surrounded by closed curves that result from intersections of invariant tori with the cut-section, then the normal mode is orbitally stable. On the contrary, if the mode appears as a saddle point, then it is orbitally unstable.

Before proceeding with numerical results, a note of caution is appropriate. The outlined stability methodology is only valid for small values of energies h. This is because, in general, the two-DOF non-linear oscillator will not possess a second independent integral of motion and hence it will not be integrable. For such non-integrable two-DOF systems, the KAM (Kolmogorov–Arnold–Moser) theory predicts that "rational" tori break, resulting in layers of ergodic motion, filling the phase space between sufficiently "irrational" preserved tori [16, 17]. As the energy increases, one typically expects all the tori to break, resulting in the filling of the whole-phase space of the system with ergodic motion.

Imposing conditions (4), (5), for the specific oscillator under investigation, one obtains

$$\dot{x}_1 = \pm[2h - \tfrac{1}{2}(1 + K)x_2^4 - x_2^2 - \dot{x}_2^2]^{1/2}. \tag{7}$$

Equations (3) and (7) define the Poincaré map for the system. The points of the Poincaré map fill the interior of a region with boundary

$$2h = \tfrac{1}{2}(1 + K)x_2^4 + x_2^2 + \dot{x}_2^2 \tag{8}$$

corresponding to the condition $\dot{x}_1 = 0$. The plan is to integrate numerically the differential equations of motion of the system and to sample the values of $(x_2, \dot{x}_2)$ corresponding to

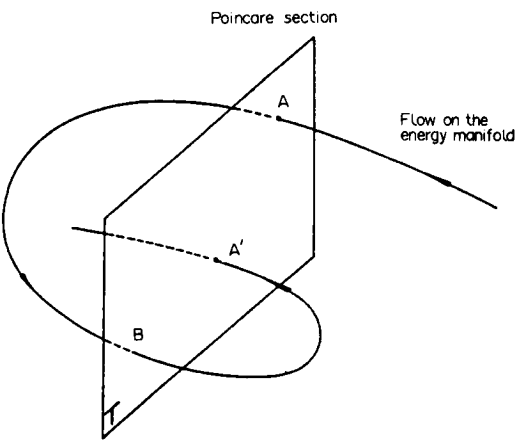

Fig. 2. Construction of the Poincaré map.

$x_1 = 0, \dot{x}_1 > 0$. In what follows, the Poincaré maps of the free oscillation of the system will be constructed and the global picture of the dynamics of the oscillator will be obtained.

3. GLOBAL DYNAMICS FOR LOW ENERGIES

3.1. *Numerical simulations*

The oscillator described by the equations of motion (1) was examined in previous works [7, 12, 15, 18] and it was found that for weak values of the coupling stiffness, a bifurcation of similar normal modes exists. To study this bifurcation, a modal relation of the form $x_2 = cx_1$ was substituted into the equations of motion (1), and the coefficients of the cubic terms in the two equations were subsequently matched. The resulting values of c depended on the ratio of the cubic terms of the coupling and end stiffnesses, as shown in Fig. 3.

It can be seen that depending on the specific value of K, two or four similar normal modes exist. Moreover, a linearized stability analysis indicates that a pitchfork bifurcation occurs at the point where the antisymmetric mode ($c = -1$) becomes unstable, and the two stable bifurcating modes are generated [7]; however, the linearized stability analysis cannot predict the stability of the in-phase (symmetric) mode (corresponding to $c = +1$) [7, 12, 15, 18]. The stability of this mode will be now investigated using Poincaré maps.

The Poincaré maps of free oscillation of the system are shown in Fig. 4. The total energy of the system, h, is fixed to a small value $h = 0.4$, and two values of the parameter K are considered: one above and one below the bifurcation value of $K = 1/4$. The following remarks can be made as far as these plots are concerned:

— The symmetric normal mode (the upper fixed point in both maps) is orbitally stable. This is concluded from the fact that it appears as a center in the plots, surrounded by closed curves which are intersections of invariant tori with the Poincaré section. Thus, the problem of the stability of the symmetric mode which could not be resolved by the linearized stability analysis, is answered by using these maps.

— A qualitative change of the global flow of the system occurs as the parameter K is decreased below the value $K = 1/4$. For $K > 1/4$ the antisymmetric mode (the lower fixed point in the Poincaré plot) is orbitally stable. For $K < 1/4$ the mode becomes orbitally unstable (since it appears as a saddle point in the plots), whereas the bifurcating modes are orbitally stable. Note the closed "loop" starting and ending at the unstable mode (in fact, there are two such "loops", but the second is difficult to observe since it is very close to the boundary curve of the plot). This path is a "homoclinic orbit" and is formed by trajectories that approach the saddle point after an infinite number of positive and negative iterations (points on the homoclinic orbit have the same past and future). The homoclinic orbit is formed when the stable and unstable invariant manifolds of the unstable point, coalesce

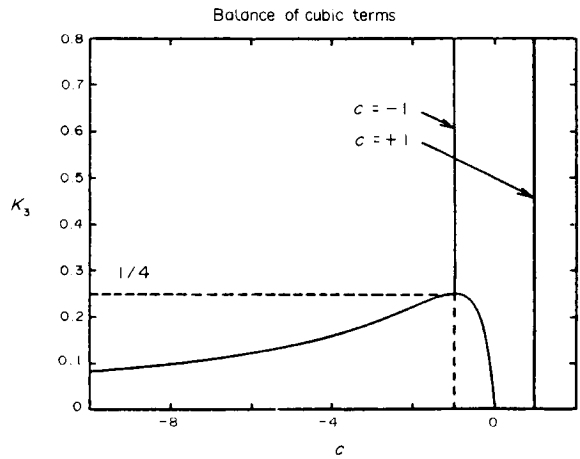

Fig. 3. Pitchfork bifurcation of normal modes. (——) stable mode, (- - - -) unstable mode.

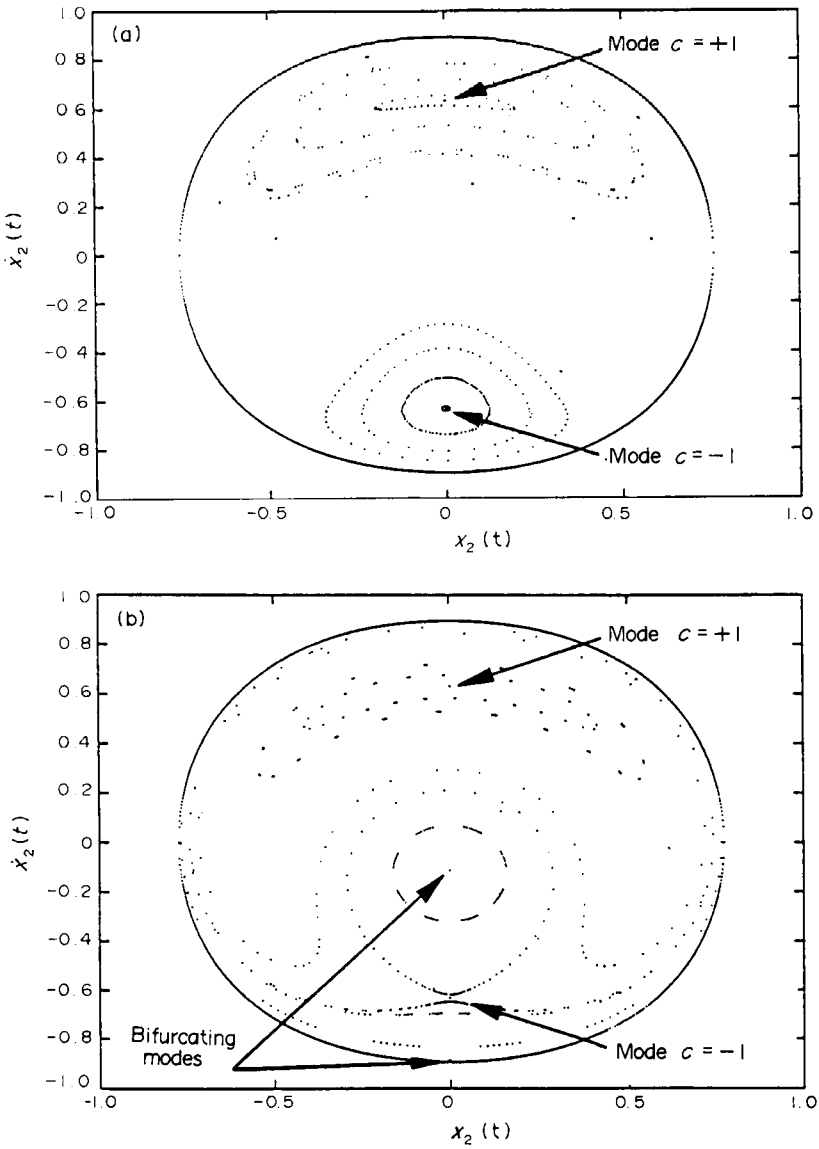

Fig. 4. Numerical Poincaré maps for a low level of energy ($h = 0.4$). (a) $K = 0.4 > 1/4$; (b) $K = 0.1 < 1/4$.

[16, 19], and it represents the boundary between trajectories that enclose only one of the bifurcating centers and those that enclose both. The homoclinic orbits are recognized as a mechanism for generation of chaos in Hamiltonian systems, and it will be shown in latter sections that for this oscillator, the observed homoclinic trajectories give rise to large-scale chaotic motion.

— As a last remark, note that the Poincaré plots correspond to a low value of the energy h. In fact, these plots can be deceiving, since they may lead to the impression that the dynamics of the oscillator are "smooth" and totally predictable. In fact, since the oscillator under investigation is *not integrable*, certain invariant tori of the flow "break" according to the KAM theorem, giving rise to random-like chaotic motions. The resulting complicated trajectories are studied in [1].

In what follows, a two-timing perturbation analysis will be used to study the dynamics of the system for low energies, and to compute analytically the various trajectories of free oscillation that are observed in the numerical simulations.

3.2. *Analytical results: averaging analysis*

In order to apply the perturbation expansion of this section, one must assume that the non-linear system "neighbors" a linear one (thus, that the non-linear solution is a perturbation of a linear one). This is the case of an oscillator with cubic, "weak" non-linearities (of perturbation order), and equations of motion of the form:

$$\ddot{x}_1 + x_1 + \varepsilon x_1^3 + \varepsilon K(x_1 - x_2)^3 = 0 \tag{9a}$$

$$\ddot{x}_2 - \varepsilon K(x_1 - x_2)^3 + \varepsilon x_2^3 + x_2 = 0 \tag{9b}$$

where $|\varepsilon| \ll 1$, is a small parameter. At this point, the additional parameter μ is introduced, defined by the relation,

$$K = \tfrac{1}{4} - \mu. \tag{10}$$

Note that μ is a measure of the distance of K from its bifurcation value of 1/4 (μ is assumed to be a non-negative quantity). At $\mu = 0$ the pitchfork bifurcation occurs, and for positive values of μ, two bifurcating normal modes exist.

The two-timing perturbation method will be implemented (for more information about this method see [20–23]). Since the system exhibits the exact similar normal mode solutions $x_1 = \pm x_2$, we begin by replacing x_1 and x_2 by new dependent coordinates u, v as follows:

$$u = (x_1 + x_2)/2, \qquad v = (x_1 - x_2)/2 \tag{11}$$

and "slow" and "fast" time variables are defined:

$$\eta = \varepsilon t, \qquad \xi = t. \tag{12}$$

Then, expressing the time derivatives of u and v by the chain rule, one obtains

$$u_t = u_\xi + \varepsilon u_\eta + O(\varepsilon^2), \qquad u_{tt} = u_{\xi\xi} + 2\varepsilon u_{\xi\eta} + O(\varepsilon^2). \tag{13}$$

Writing the equations of motion (9) in terms of the new variables u and v and using expressions (13), the following approximate transformed equations of motion result (correct to $O(\varepsilon^2)$):

$$u_{\xi\xi} + u = -2\varepsilon u_{\xi\eta} - 3\varepsilon u v^2 - \varepsilon u^3 + O(\varepsilon^2) \tag{14a}$$

$$v_{\xi\xi} + v = -2\varepsilon v_{\xi\eta} + 8\varepsilon\mu v^3 - 3\varepsilon v^3 - 3\varepsilon u^2 v + O(\varepsilon^2). \tag{14b}$$

In these equations the "subscript" notation for the derivatives was used, for example, $(\cdot)_{\xi\eta} \equiv \dfrac{\partial^2(\cdot)}{\partial\xi\partial\eta}$. Note that all variables other than ε are assumed to be of $O(1)$. The solutions of equations (14) are expressed in the series form:

$$u(\xi, \eta) = \sum_{n=0}^{\infty} \varepsilon^n u_n(\xi, \eta) \tag{15a}$$

$$v(\xi, \eta) = \sum_{n=0}^{\infty} \varepsilon^n v_n(\xi, \eta) \tag{15b}$$

where u_n, v_n are the nth-order approximations to the solution. These are computed by substituting the series expressions for u and v into equations (14), and matching coefficients of respective powers of ε.

The zeroth-order approximate solutions are given by the following set of differential equations:

$$u_{0\xi\xi} + u_0 = 0 \tag{16a}$$

$$v_{0\xi\xi} + v_0 = 0. \tag{16b}$$

The general solutions of these equations are of the form:

$$u_0(\xi, \eta) = A(\eta)\cos\xi + B(\eta)\sin\xi \tag{17a}$$

$$v_0(\xi, \eta) = C(\eta)\cos\xi + D(\eta)\sin\xi \tag{17b}$$

where the (unknown) quantities A, B, C and D are computed by eliminating the "secular" terms of the equations of the next approximation [20].

The equations of the first approximation are obtained by matching terms of order ε:

$$u_{1\xi\xi} + u_1 = -2u_{0\xi\eta} - 3u_0 v_0^2 - u_0^3 \tag{18a}$$

$$v_{1\xi\xi} + v_1 = -2v_{0\xi\eta} + 8\mu_0 v_0^3 - 3v_0^3 - 3u_0^2 v_0. \tag{18b}$$

Substituting the expressions for u_0 and v_0 into the left-hand sides of equations (18) and setting to zero the coefficients of $\cos\xi$ and $\sin\xi$ and (since they represent resonant excitations for the system (18) leading to unbounded solutions), one obtains four differential equations for the unknown quantities A, B, C and D. This operation was performed with the symbolic manipulation software package MACSYMA and the expressions are too lengthy to be reported here. However, the results can be significantly simplified if one uses a new set of polar coordinates, $R_1(\eta)$, $R_2(\eta)$, and $\phi(\eta)$, defined by

$$A = R_1 \cos\theta_1, \qquad B = R_1 \sin\theta_1, \qquad C = R_2 \cos\theta_2,$$
$$D = R_2 \sin\theta_2, \qquad \phi = \theta_2 - \theta_1. \tag{19}$$

In terms of these new variables, the equations that result from the elimination of the secular terms of equations (18), are as follows:

$$\frac{dR_1}{d\eta} = \tfrac{3}{8} R_1 R_2^2 \sin 2\phi$$

$$\frac{dR_2}{d\eta} = -\tfrac{3}{8} R_1^2 R_2 \sin 2\phi$$

$$\frac{d\phi}{d\eta} = -\tfrac{3}{8}(R_1^2 + R_2^2) + 3\mu R_2^2 + \tfrac{3}{8}(R_2^2 - R_1^2)\cos 2\phi \tag{20}$$

where the variable ϕ is modulo π. Combining the first two equations of the above set, one obtains

$$\frac{dR_1}{dR_2} = -\frac{R_2}{R_1} \Rightarrow R_1^2 + R_2^2 = \rho^2 \tag{21}$$

where ρ is a constant scalar quantity. Note that the quantity $(R_1^2 + R_2^2)$ is related to the total energy of the motion; thus, expression (21) indicates that the total energy of the system is conserved during free oscillation (as expected). Note, however, that this form of the conservation law holds only for this level of approximation, since terms of order ε^2 or higher are not taken into account.

Equations (20) represent a dynamical system with a three-dimensional phase space. However, since the energy is fixed during free oscillation, the motion of the dynamical system is confined to a two-dimensional isoenergetic manifold, represented by the cylindrical surface of Fig. 5. In that figure, a schematic description of the flow of the dynamical system is given for $\mu > 0$ (the pitchfork bifurcation of modes has already occurred). The variable ϕ is confined to the range $[0, \pi)$, and the plot is symmetric with respect to the plane $\phi = \pi/2$. Points that are symmetric with respect to that plane must be identified since they represent the same motion of the dynamical system (this is due to the applied mathematical transformations).

The antisymmetric mode corresponds to $R_1 = 0, R_2 = \rho$ and thus appears in Fig. 5 as a straight-line through points A and A′. (If we identify $\phi = 0$ with $\phi = \pi$, it becomes a closed curve.) The polar transformation (19) has "blown up" the point $R_1 = 0$ into a closed curve, with each point on the curve corresponding to a direction ϕ. In particular the points A and A′ correspond to the directions at which the homoclinic orbit approaches the saddle. Similarly, the two additional bifurcating modes are represented by the fixed points B and C, and are centers, indicating orbital stability.

The motion on the isoenergetic manifold can be better described if one introduces a second polar transformation according to the formulas:

$$R_1 = \rho \cos\psi \tag{22a}$$

$$R_2 = \rho \sin\psi \tag{22b}$$

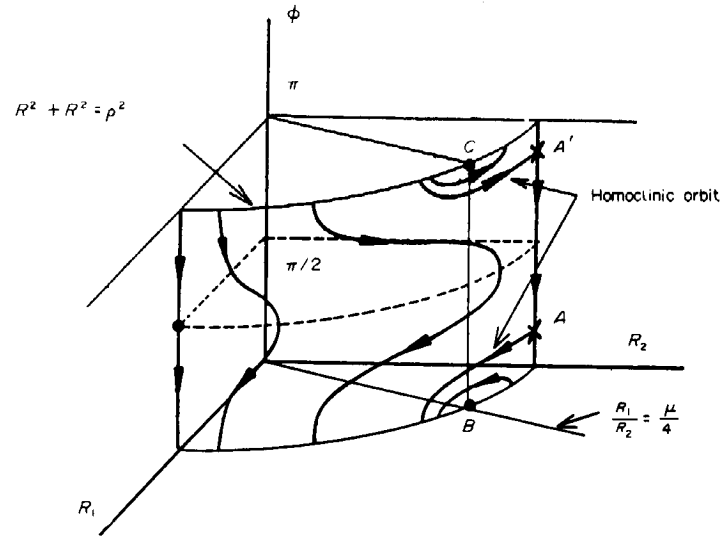

Fig. 5. Schematic representation of the averaged flow on the isoenergetic manifold (positive μ).

where ρ is the scalar energy constant defined in equation (21), and ψ is a new polar variable. Substituting expressions (22) into equations (20) and eliminating the constant ρ, one obtains the following set of differential equations that describe the free oscillation of the system on the isoenergetic manifold:

$$\frac{d\phi}{d\eta} = -\frac{3\rho^2}{16}[8\mu(\cos 2\psi - 1) + 2 + 2\cos 2\psi \cos 2\phi]$$

$$\frac{d\psi}{d\eta} = -\frac{3\rho^2}{16}\sin 2\phi \sin 2\psi$$

$$\rho = \text{constant}. \tag{23}$$

Note that the above equations represent a dynamical system on a two-torus, since the variables ϕ and ψ are modulo π. Thus, by applying subsequent transformations, one finally relates the free oscillation of the two-DOF system with a flow of a vector field on a two-torus.

An interesting feature of equations (23) is that they can be integrated exactly. Indeed, the integrating factor for this system of ordinary differential equations is

$$F(\phi, \psi) = \sin 2\psi \tag{24}$$

and the first integral of motion is computed as

$$K(\phi, \psi) = -\tfrac{1}{2}\sin^2 2\psi \cos 2\phi + (1 - 4\mu)\cos 2\psi + \mu \cos 4\psi. \tag{25}$$

The level curves of the integral (25) (corresponding to solutions of equations (23)) are plotted in Fig. 6 for $\mu = 0.05$. Each curve corresponds to a different value for the integral K, but all are on the same "energy level" ρ. Observe that the flow on the torus is symmetric with respect to the lines $\phi = \pi/2$ and $\psi = \pi/2$. The symmetric mode corresponds to $(\phi, \psi) = (\pi/2, 0)$ and appears to be surrounded by closed curves. This is an analytic proof of the orbital stability of the symmetric mode (cf. [15]). Recall that a numerical proof was obtained with Poincaré maps, where it was found that the symmetric mode was surrounded by closed curves that result as intersections of invariant tori with the cut plane. The two bifurcating modes are orbitally stable (since they appear as centers) and correspond to the fixed points $(\phi, \psi) = \left(0, \tfrac{1}{2}\cos^{-1}\left(\frac{4\mu - 1}{4\mu + 1}\right)\right)$ and $\left(\pi, \tfrac{1}{2}\cos^{-1}\left(\frac{4\mu - 1}{4\mu + 1}\right)\right)$, respectively. Finally, the unstable antisymmetric normal mode is represented by the fixed points

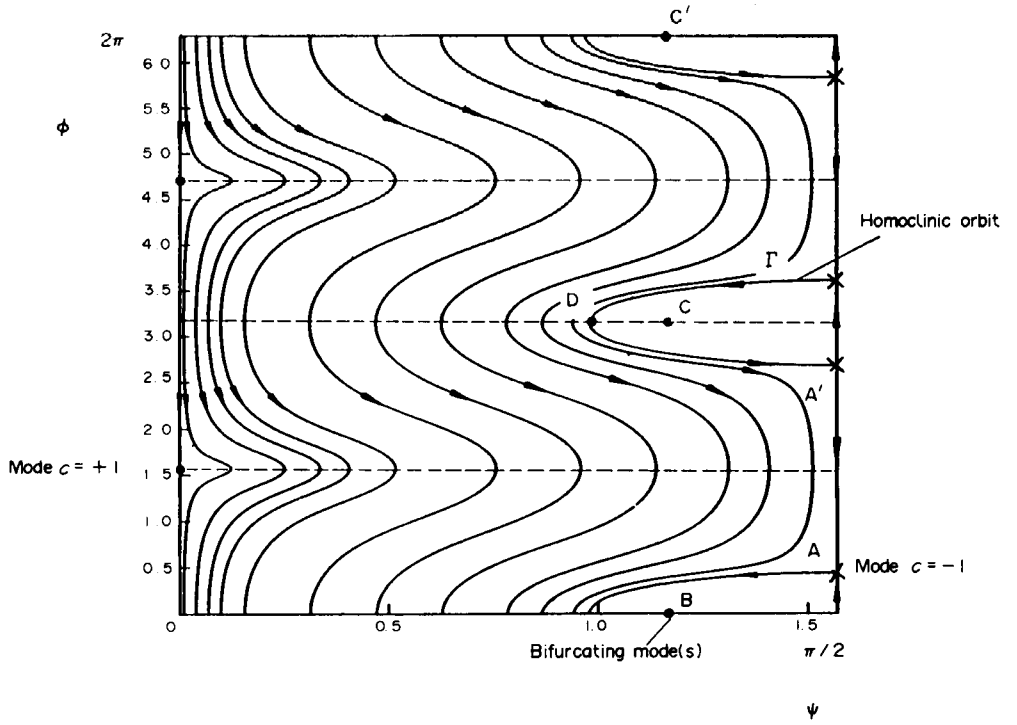

Fig. 6. Averaged flow on the 2-torus, $\mu = 0.05$.

$(\phi, \psi) = \left(\frac{1}{2}\cos^{-1}(1-8\mu), \frac{\pi}{2}\right)$ and $\left(\pi - \frac{1}{2}\cos^{-1}(1-8\mu), \frac{\pi}{2}\right)$. Note that the homoclinic orbit Γ appears as an open curve. In previous works [7, 18] it was reported that for the "1–1 resonant" system (i.e. the system with equal linearized eigenvalues), the two bifurcating modes actually represent the same free oscillations. Exactly the same conclusion can be made from the phase plane of Fig. 7, if one identifies points symmetric with respect to line $\phi = \pi/2$: the two bifurcating modes represent actually the same motion and in addition, the homoclinic orbit originates from and ends at the unstable mode.

In Fig. 7, the phase plane of the oscillator for different values of μ is shown (only values of ϕ and ψ between 0 and $\pi/2$ are presented). Observe that at $\mu = 0$ only the symmetric and antisymmetric modes exist. As μ is increased from zero, the homoclinic orbit increases in length. At the limit $\mu = 1/4$, the coupling stiffness of the oscillator vanishes and the two-DOF system degenerates into two single-DOF disjoint oscillators. Note that as $\mu \to 0, 1/4$, the homoclinic orbit becomes more and more "curved", until it reaches non-smooth limits.

The analytical expressions of the perturbation analysis can be used to construct Poincaré maps similar to those that were computed earlier [Fig. 4(a, b)]. This can be done by expressing the perturbation results (17)–(25) in terms of the "old" coordinates x_1 and x_2; details of this procedure can be found in the Appendix. The approximate Poincaré maps corresponding to $K = 0.15$ and 0.4, and to energy $h = 0.5$ appear in Fig. 8(a) and (b); it can be seen that they are similar to those obtained by a direct integration of the equations of motion [Fig. 4(a, b)]. Thus, it is verified that the approximate perturbation analysis indeed captures the low-energy dynamics of the system under consideration.

By using the analytic expression of the first integral of motion (equation (25)), it is possible to find exact expressions for the time responses of the coordinates of the oscillator. In the following, the time responses corresponding to a homoclinic motion of the system will be computed. The value of $K(\phi, \psi)$ for the homoclinic level curve, is obtained by substituting $\phi = \frac{1}{2}\cos^{-1}(1-8\mu)$, $\psi = \pi/2$ into equation (25) and is given by

$$K(\phi, \psi) = 5\mu - 1 \quad \text{(homoclinic orbit)}. \tag{26}$$

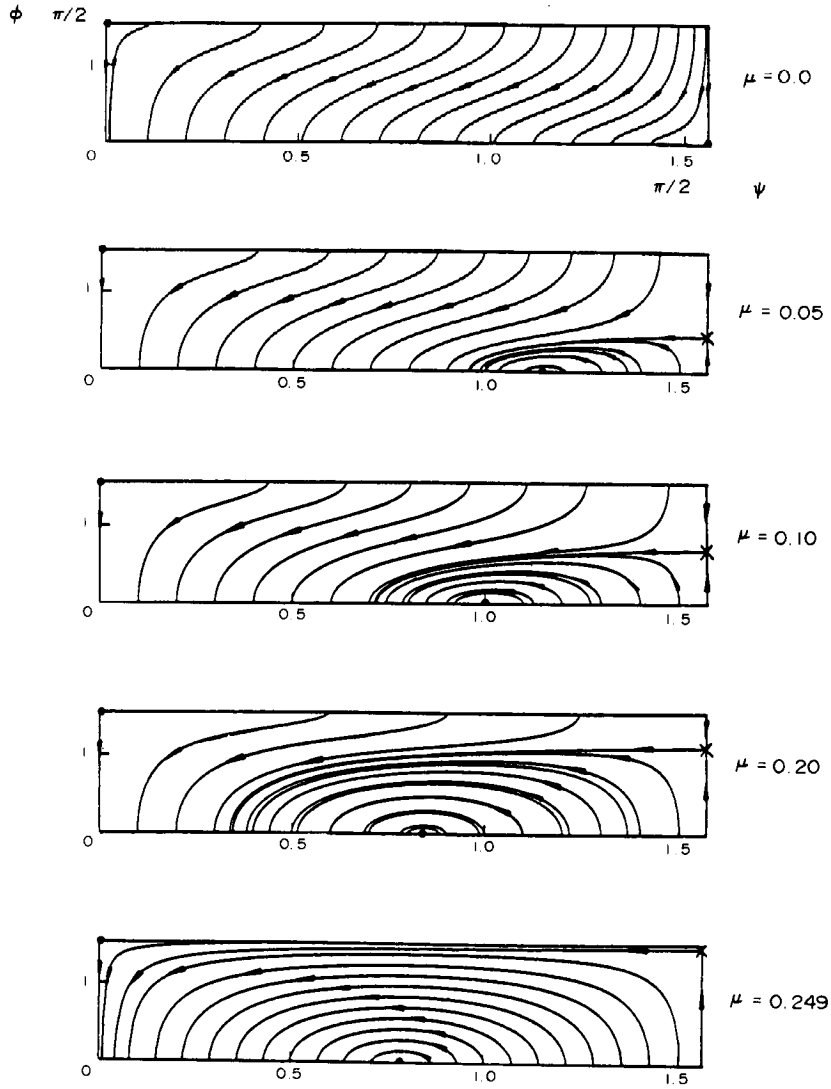

Fig. 7. Phase plane of the averaged flow for increasing μ.

Using this value of K, one finds the following relation between ϕ and ψ for a motion on the homoclinic orbit (this is achieved by solving for $\cos 2\phi$ in expression (25)):

$$\cos 2\phi = \frac{2 - 10\mu + 2(1 - 4\mu)\cos 2\psi + 2\mu \cos 4\psi}{\sin^2 2\psi} \quad \text{(homoclinic orbit).} \tag{27}$$

Using expression (27), one can eliminate the variable φ from the second of equations (23), to obtain the following differential equation for ψ:

$$\frac{d\psi}{d\eta} = \frac{3\rho^2}{16}\left\{\frac{[(12\mu - 1) + (8\mu - 2)\cos 2\psi - (4\mu + 1)\cos^2 2\psi]}{\sin^2 2\psi}\right.$$
$$\left.\cdot[(3 - 12\mu) + (2 - 8\mu)\cos 2\psi + (4\mu - 1)\cos^2 2\psi]\right\}^{1/2} \tag{28}$$

where the upper $(-)$ and lower $(+)$ signs are used for $\phi \in [0, \pi/2)$ and $[\pi/2, \pi)$, respectively. Introducing a new dependent variable, $x = \cos 2\psi$, the differential equation (28) can be written in the following simplified form:

$$\frac{Q_1\, dx}{[(A_1 + B_1 x - x^2)(3 + 2x - x^2)]^{1/2}} = \pm d\eta \tag{29}$$

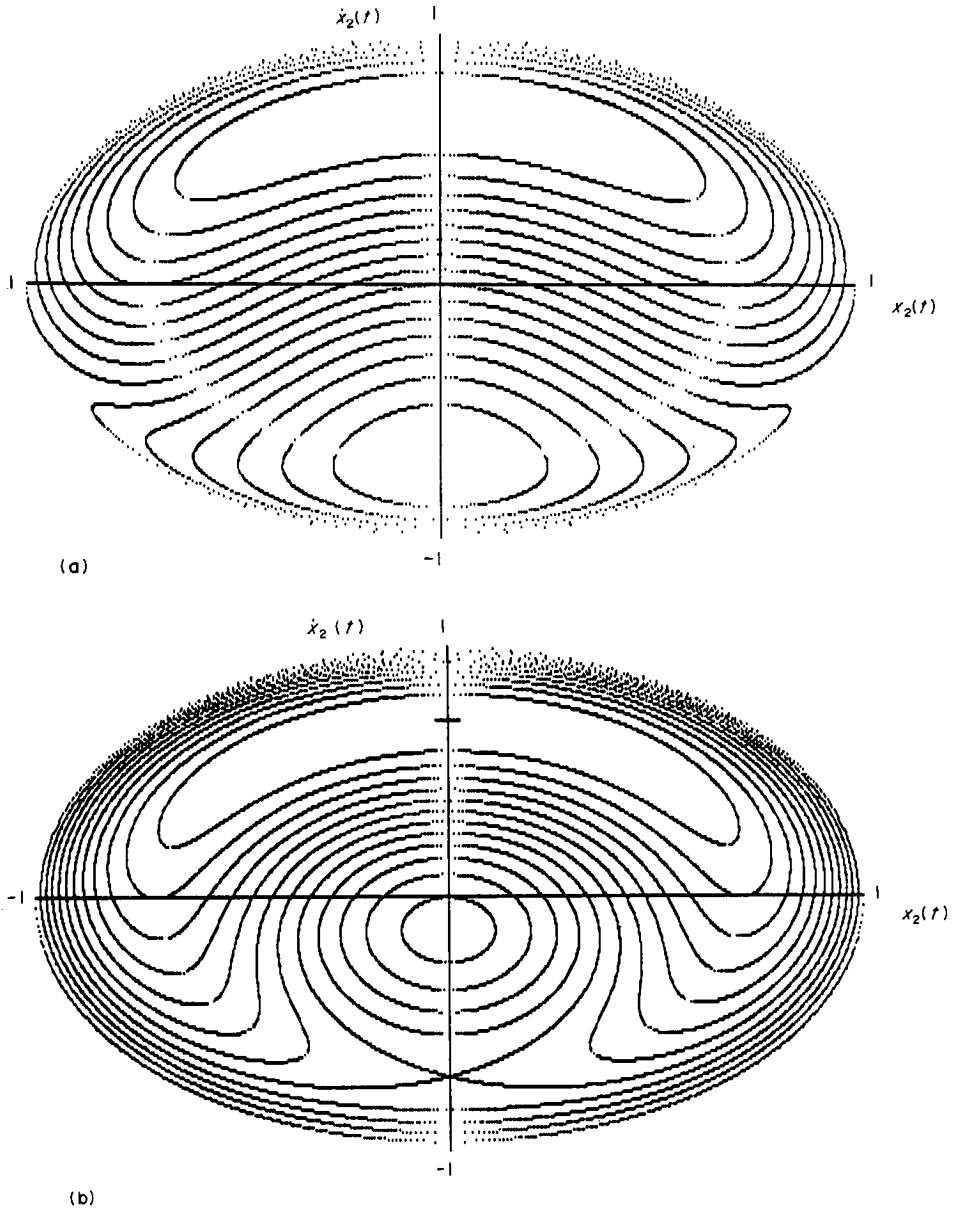

Fig. 8. Poincaré maps derived by perturbation analysis for a low level of energy ($h = 0.5$). (a) $K = 0.4 > 1/4$; (b) $K = 0.1 < 1/4$.

where

$$Q_1 = \frac{8}{3\rho^2(1-16\mu^2)^{1/2}}, \qquad A_1 = \frac{12\mu - 1}{4\mu + 1}, \qquad B_1 = \frac{8\mu - 2}{4\mu + 1}.$$

Equation (29) can be integrated formally by quadratures as follows. Assume that at $\eta = 0$ (or equivalently at time $t = 0$), the system is at position $(\phi, \psi) = \left(\pi, \tfrac{1}{2}\cos^{-1}\left(\frac{12\mu - 1}{4\mu + 1}\right)\right)$ i.e. at point D of the phase plane of Fig. 6. Then, arbitrary (positive or negative) values of η are obtained by performing an integration of expression (29) with the following limits:

$$\int_{(12\mu-1)/(4\mu+1)}^{x} \frac{Q_1\,d\xi}{[A_1 + B_1\xi - \xi^2)(3 + 2\xi - \xi^2)]^{1/2}} = \pm\int_0^{\eta} d\tau = \pm\eta. \tag{30}$$

Fortunately, the associated integrals can be found in standard tables [24], so that the final result of the above integration can be analytically expressed in terms of elementary

functions as

$$\frac{16\mu^{1/2}}{(1+4\mu)^{1/2}}\left[1-\frac{4(8\mu+1)}{(4\mu+1)(x+1)}+\frac{64\mu}{(4\mu+1)(x+1)^2}\right]^{1/2}+\frac{128\mu}{(4\mu+1)(x+1)}$$
$$=\frac{32\mu+4}{4\mu+1}+\frac{4}{4\mu+1}\exp\left(\pm\{-3\eta[\mu(1-4\mu)]^{1/2}\rho^2\}\right). \tag{31}$$

Equation (31) gives the relation between the variables η and x (or equivalently t and ψ) for the motion on the homoclinic orbit. Certain remarks can be made as far as the above expression is concerned.

— This complicated expression represents a solution for the homoclinic motion that is correct only up to $O(\varepsilon^2)$, for times only up to $(1/\varepsilon)$. Moreover, one can easily express the slow-time variable η as a function of x (and thus ψ), by rearranging terms and taking the logarithms of both sides of the equation. Note that η (the time-like variable) appears as an exponent of an exponential function. This is typical of time responses on homoclinic orbits, since as discussed earlier the motions on the homoclinic trajectory approach asymptotically the same limit for positive or negative infinite times.

— The upper (+) sign corresponds to $\phi\in[0,\pi/2)$, and gives negative values for η that decrease as x increases. Moreover, as x approaches the limiting value $x=\cos 2\psi=-1$ (corresponding to the antisymmetric mode), one obtains

$$\lim_{x\to -1}\eta=-\infty\,(\phi\in[0,\pi/2)).$$

This result confirms that the motion on the homoclinic orbit originates from the antisymmetric normal mode (since it approaches this state of motion for negative infinite times).

— Similarly, the lower (−) sign is used when $\phi\in[\pi/2,\pi)$, and results in positive values of η. One finds that η increases as x increases, reaching the limit,

$$\lim_{x\to -1}\eta=+\infty\,(\phi\in[0,\pi/2,\pi))$$

which implies that the motion reaches the antisymmetric mode for infinite positive times (as expected).

— The solution (31) is an approximation to the homoclinic motion for low energies of the system. When the level of energy is increased, the stable and unstable invariant manifolds comprising the homoclinic orbit intersect transversely and Smale horseshoes are formed, leading to chaotic motions [1]. Unfortunately, one cannot use the exact solution of this section as a basis for a homoclinic Melnikov analysis [16], since the resulting Melnikov functions become exponentially small as $\varepsilon\to 0$. To show this, consider the dynamical system:

$$\dot{x}=\varepsilon f(x)+\varepsilon^2 f_1(x,t),\quad x\in R^2$$

where the system $\dot{x}=\varepsilon f(x)$ is Hamiltonian (the perturbation $f_1(x,t)$ need not be Hamiltonian). Rescaling the time variable $t\to t/\varepsilon$, the system can be written as

$$\dot{x}=f(x)+\varepsilon f_1(x,t/\varepsilon).$$

Assuming that the unperturbed Hamiltonian system (the first term in the above equation) contains a homoclinic orbit, the above dynamical system is equivalent to the one described by the averaged equations that were obtained by the two-variable method. Applying homoclinic Melnikov analysis for the perturbed system, one obtains a Melnikov function which *explicitly depends on the perturbation parameter* ε:

$$M(t_0/\varepsilon)=\int_{-\infty}^{\infty}\{f[q^0(t)],f_1[q^0(t),(t+t^0)/\varepsilon]\}\,dt$$

where $\{\cdot,\cdot\}$ is the Poisson bracket. Considering the above Melnikov function, it can be shown that [16]:

$$\max_{t_0\in[0,T]} M(t_0/\varepsilon)\sim e^{-c/\varepsilon}$$

and the Melnikov function becomes exponentially small as the perturbation parameter diminishes. Although one cannot prove analytically the existence of transverse homoclinic intersections, this can be proven numerically, by computing the stable and unstable invariant manifolds of the unstable antisymmetric normal mode [1].

4. DISCUSSION

The low-energy free oscillations of a strongly non-linear, discrete, Hamiltonian oscillator with cubic non-linearity were examined. This oscillator has a potential function that is symmetric with respect to the origin of the configuration space, and it possesses normal modes of free oscillation, analogous to the ones observed in linear systems.

The global dynamics of the oscillator were studied by means of numerical and analytical Poincaré maps. For low energies, the dynamics of the system appear to be smooth and totally predictable. In fact, it was shown that a two-timing perturbation technique can approximately describe any possible low-energy motion.

A basic feature of the low-energy map is the existence of a homoclinic orbit. This trajectory occurs only after the bifurcation of normal modes has taken place, i.e. for "weak coupling" ($K < 1/4$), and results from the identification of the stable and unstable manifolds of the unstable antisymmetric normal mode. The importance of this homoclinic orbit will be discussed in a companion paper [1] where it will be shown that it gives rise to large-scale chaotic free trajectories. For a system with $K > 1/4$ ("strong coupling") no such homoclinic orbit is possible since both similar modes are orbitally stable. The only possible high-energy chaotic motions in that case result from the breakdown of the rational tori of the system and are thus localized in small areas of the phase plane.

A general result of this work is that bifurcations of the normal modes of a non-linear system greatly affect its low-energy dynamics. As shown for the specific system under consideration, the transition of a similar mode from orbital stability to orbital instability gives rise to new qualitative global dynamic phenomena which greatly enrich the low-energy global dynamics.

Acknowledgements—The first author wishes to thank Prof. T. Caughey of the California Institute of Technology for stimulating discussions and helpful insight on several aspects of this work. The authors would also like to thank J. M. Sivo of the California Institute of Technology for his help in the construction of the numerical Poincaré maps.

REFERENCES

1. A. Vakakis and R. Rand, Normal modes and global dynamics of a two degree of freedom nonlinear system—II. High energies. *Int. J. Non-Linear Mech.* **27**, 875–888 (1992).
2. M. Liapounov, *The General Problem of the Stability of Motion.* Princeton University Press, Princeton, NJ (1947).
3. A. Weinstein, Normal modes for nonlinear Hamiltonian systems. *Inventiones Math.* **20**, 47–57 (1973).
4. R. Rosenberg, The normal modes of nonlinear *n*-DOF systems. *J. appl. Mech.* **30**, 7–14 (1962).
5. R. Rosenberg, On a geometrical method in nonlinear vibrations. *Int. Conf. in Non-linear Vibrations*, Marseille (7–12 September 1964).
6. R. Rosenberg, On nonlinear vibrations of systems with many DOF. *Adv. appl. Mech.* **9**, 155–242 (1966).
7. T. Caughey, A. Vakakis and J. Sivo, Analytical study of similar normal modes and their bifurcations in a class of strongly nonlinear systems. *Int. J. Non-Linear Mech.* **25**(5), 521–533 (1990).
8. R. Rand, A direct method for nonlinear normal modes. *Int. J. Non-linear Mech.* **9**, 363–368 (1974).
9. T. Johnson and R. Rand, On the existence and bifurcation of minimal normal modes. *Int. J. Non-Linear Mech.* **14**, 1–12 (1979).
10. C. Pak, On the stability behavior of bifurcated normal modes in coupled nonlinear systems. *J. appl. Mech.* **56**, 155–161 (1989).
11. D. Yen, On the normal modes of nonlinear dual-mass systems. *Int. J. Non-Linear Mech.* **9**, 45–53 (1974).
12. L. Month and R. Rand, The stability of bifurcating periodic solutions in a two DOF non-linear system. *J. appl. Mech.* 782–783 (1977).
13. M. Hyams and L. Month, The origin of stability indeterminacy in a symmetric Hamiltonian. *J. appl. Mech.* **51**, 399–405 (1984).
14. L. Month, On approximate first integrals of Hamiltonian systems with an application to non-linear normal modes in a two DOF oscillator. PhD thesis, Cornell University Press, Ithaca (1979).
15. L. Month and R. Rand, An application of the Poincaré map to the stability of nonlinear normal modes. *J. appl. Mech.* **47**, 645–651 (1980).
16. J. Guckenheimer and P. Holmes, *Non-linear Oscillations, Dynamical Systems, and Bifurcations of Vector Fields.* Springer, Berlin (1984).
17. A. Lichtenberg and M. Lieberman, *Regular and Stochastic Motions.* Springer, Berlin (1983).

18. A. Vakakis, Analysis and identification of linear and nonlinear normal modes in vibrating systems. Ph.D. thesis, California Institute of Technology (1990).
19. S. Wiggins, *Global Bifurcations and Chaos: Analytical Methods*. Springer, Berlin (1989).
20. R. Rand and D. Armbruster, *Perturbation Methods, Bifurcation Theory and Computer Algebra*. Springer, Berlin (1987).
21. A. H. Nayfeh and D. T. Mook, *Non-linear Oscillations*. Wiley-Interscience, New York (1979).
22. A. H. Nayfeh, *Perturbation Methods*. Wiley, New York (1973).
23. J. Kevorkian and J. D. Cole, *Perturbation Methods in Applied Mathematics*. Springer, New York (1981).
24. P. Byrd and D. Friedman, *Handbook of Elliptic Integrals for Engineers and Physicists*. Springer, Berlin (1954).

APPENDIX: COMPUTATION OF APPROXIMATE POINCARÉ MAPS USING THE TWO VARIABLE PERTURBATION ANALYSIS

The variables x_1 and x_2 of the equations of motion (9), can be related to the variables u and v of the perturbation analysis by "inverting" equations (11) as follows:

$$x_1 = u + v, \qquad x_2 = u - v. \tag{A1}$$

To construct the Poincaré map, one must set $x_1 = 0$, or taking into account (A1):

$$x_1 = u_0 + v_0 = 0 + O(\varepsilon). \tag{A2}$$

Substituting expressions (17) in to expression (A2), one finds the following expression for the variable ξ:

$$\tan\xi = -[C(\eta) + A(\eta)]/[D(\eta) + B(\eta)]. \tag{A3}$$

Using equations (A3), (17) and the second of equations (A1), the following expression for x_2 is obtained:

$$x_2 = 2(BC - AD)/(D^2 + 2BD + C^2 + 2AC + B^2 + A^2)^{1/2} \tag{A4}$$

where the argument η from $A, B, \ldots$ was omitted. The variable x_2 is one of the two variables necessary for the construction of the Poincaré map. The other is the velocity $\dot{x}_2$, which to lowest order in ε is given by $dx_2/d\xi$. Using (A3) this gives:

$$\dot{x}_2 = (D^2 + C^2 - B^2 - A^2)/(D^2 + 2BD + C^2 + 2AC + B^2 + A^2)^{1/2}. \tag{A5}$$

Introducing the polar transformations (19) and (22), equations (A4), (A5) take the form:

$$x_2 = \rho\sin\phi\,\sin 2\psi/(1 + \cos\phi\,\sin 2\psi)^{1/2}, \qquad \dot{x}_2 = \rho\cos 2\psi/(1 + \cos\phi\,\sin 2\psi)^{1/2}. \tag{A6}$$

In order to create the Poincaré map, one must use the first integral (25) and for given values of μ, K, ρ and ψ, solve for $\cos 2\phi$. Plugging the obtained values of ϕ into equations (A6), one can evaluate x_2 and $\dot{x}_2$ and then plot them to construct the Poincaré map. The total energy h of the system (used for constructing the numerical plots of Fig. 4) is related to the variable ρ of the perturbation analysis by the expression:

$$h = \rho^2. \tag{A7}$$